Modelling of HNO3-mediated laser-induced condensation: A parametric study

P. Rohwetter, J. Kasparian, L. Wöste, and J.-P. Wolf

Citation: The Journal of Chemical Physics **135**, 134703 (2011); doi: 10.1063/1.3644591
View online: http://dx.doi.org/10.1063/1.3644591
View Table of Contents: http://scitation.aip.org/content/aip/journal/jcp/135/13?ver=pdfcov
Published by the AIP Publishing

Modelling of HNO_3-mediated laser-induced condensation: A parametric study

P. Rohwetter,[1] J. Kasparian,[2,a)] L. Wöste,[1] and J.-P. Wolf[2]
[1]*Teramobile, Institut für Experimentalphysik, Freie Universität Berlin, Arnimallee 14, D 14195 Berlin, Germany*
[2]*Teramobile, Université de Genève, GAP-Biophotonics, 20 rue de l'Ecole de Médecine, 1211 Geneva 4, Switzerland*

(Received 29 July 2011; accepted 9 September 2011; published online 3 October 2011)

Based on both static (extended Köhler) and dynamic modelling, we investigate the influence of temperature, humidity, HNO_3 initial concentration, as well as of the particle concentration, on the efficiency of HNO_3-mediated laser-induced condensation. This mechanism is most efficient for low temperatures, high HNO_3 concentration, and relative humidities. It is, however, still active up to 30 °C, down to 70% relative humidity, and below the ppm level of HNO_3. Furthermore, lower particle concentration minimizing the depletion of both HNO_3 and water vapor is more favourable to particle growth. © *2011 American Institute of Physics*. [doi:10.1063/1.3644591]

I. INTRODUCTION

Self-guided filaments[1–4] generated by ultrashort laser pulses have recently been proposed as candidates to trigger water condensation in the atmosphere,[5] as an alternative to the dispersion of particles such as AgI in the atmosphere.[6] Laser filaments are self-guided light structures of typically 100 μm diameter and up to hundreds of meters in length, extending widely beyond the traditional linear diffraction limit. Their formation stems from an intensity-dependent refractive index modification of the propagation medium, known as the Kerr effect, which is due to third-order nonlinear polarization of the medium. It results in the self-focusing of the beam, until the intensity rises sufficiently for ionizing the air. The self-generated plasma[1–4] and/or negative higher-order Kerr terms[7,8] then balance the self-focusing, resulting in the emergence of self-guided filaments.

Due to their typical intensity of 5×10^{13} W/cm^2, filaments generate electron concentrations of $10^{15} - 10^{16}$ cm^{-3}, and allow efficient multiphoton photo-oxidation of the air molecules. Such photo-activation of the atmosphere yields extremely high concentrations of ozone and NO_2 gases. They reach up to 10^{16} and 3×10^{15} cm^{-3}, respectively, leading to HNO_3 concentrations in the ppm-range within the 100 μm thin filament volume.[9] Such extremely high concentration (1000–10 000 times the typical natural atmospheric concentration[10]) of this hygroscopic molecule, known to contribute to particle stabilization besides H_2SO_4 in natural conditions,[11] has recently been shown[9,12] to provide a major ingredient to the laser-induced condensation process at moderate relative humidity (RH) down to 70%, by stabilizing and sustaining the growth of otherwise evaporating particles.[5]

Field experiments confirmed this mechanism over a wide range of atmospheric conditions (2–36 °C, 35%–100% RH),[5] suggesting that it may be quite general in the presence of laser filaments. Here, based on both static modelling relying on the extended Köhler model, and dynamic modelling of the particle growth, we investigate the influence of temperature, humidity, HNO_3 initial concentration, as well as the particle concentration, on the efficiency of HNO_3-mediated laser-induced condensation. We show that this mechanism is most efficient for low temperatures, and high HNO_3 concentration and relative humidities, but is still active up to 30 °C, down to 70% relative humidity, and below the ppm level of HNO_3. Furthermore, temperature appears as the most critical parameter. Finally, lower particle concentration minimizing the depletion of both HNO_3 and water vapor is more favourable to particle growth.

II. METHODS: DESCRIPTION OF THE MODELS

A. Extended Köhler model: Particle stability assessment

The stability of particles under the conditions encountered in laser-induced condensation experiments was investigated based on the extended Köhler theory of Laaksonen *et al.*,[14] which we further adapted to describe the relevant atmospheric conditions. More specifically, we dropped the assumption of a dilute ionic solution which in particular imposes low trace gas concentrations in the atmosphere, as well as conditions close to water vapor saturation.[11] Instead, we considered a situation similar to that of stratospheric aerosols containing concentrated sulphuric acid in an atmosphere rich in gaseous HNO_3, as treated by Kokkola *et al.*[15] We checked that in spite of these modifications, our model converges back to the classical one at low HNO_3 concentrations.

The equilibrium of aqueous solution particles with an atmosphere containing a highly soluble trace gas depends on two simultaneous equilibria: $H_2O(g) \rightleftharpoons H_2O(sol)$ and $HNO_3(g) \rightleftharpoons HNO_3(sol)$, where "(sol)" and "(g)" refer to quantities in the liquid particle and in the gas phase, respectively. This double equilibrium is described by the following

a)Electronic mail: jerome.kasparian@unige.ch.

equation:

$$p_{\infty,i}(T, \boldsymbol{m}_j) = p_{\mathrm{sat},i}(T, \boldsymbol{m}_j)\, \exp\left(\frac{4\,\sigma(T_\mathrm{p}, \boldsymbol{m}_j)\, v_i(T_\mathrm{p}, \boldsymbol{m}_j)}{k_\mathrm{B}\, T\, D_\mathrm{p}(T_\mathrm{p}, \boldsymbol{m}_j)}\right), \tag{1}$$

where k_B is the Boltzmann constant, D_p the particle diameter, and the index i stands for the species H_2O or HNO_3. $p_{\infty,i}(T, \boldsymbol{m}_j)$ denotes the partial pressure of species i at a temperature T in the atmosphere, m_i its mass in the liquid phase, $p_{\mathrm{sat},i}(T, \boldsymbol{m}_j)$ its partial pressure at saturation over a flat liquid phase of same composition, as defined by the set of masses $\boldsymbol{m}_j$, $v_i(T_\mathrm{p}, \boldsymbol{m}_j)$ denotes its partial molecular volume, and $\sigma(T_\mathrm{p}, \boldsymbol{m}_j)$ is the surface tension of the solution for a particle at temperature T_p.

The set of Eq. (1), in which the exponential term results from the Kelvin effect, stems from the minimization of the Gibbs energy. Besides water and HNO_3, we consider that the liquid phase additionally contains a fully dissolved nonvolatile substance, namely NH_4NO_3 salt, a typical constituent of atmospheric water-soluble aerosol acting as germs for heterogeneous nucleation. This salt is chosen because it is sufficiently common in the troposphere[11,16] to be considered representative. Thermodynamical data about the the ternary solution of H_2O, HNO_3, and NH_4NO_3 are available from the semi-empirical Extended Aerosol Inorganics Model (E-AIM) of Clegg and co-workers[17–19] over the whole range of conditions under consideration.

We take into account the depletion of water vapor and HNO_3 from the gas phase due to their condensation into the particles, following Konopka and Vogelsberger,[13] and Laaksonen *et al.*,[14] respectively. This depletion depends on the particle density and size distribution. In this work, we assumed a fixed particle number concentration C_p and a monodisperse particle size distribution providing reasonable accuracy.[14]

The stability of the particles in given conditions was characterized by constructing the Köhler curves. In that purpose, Eq. (1) is solved while imposing the conservation of the total mass (in both gas liquid phases) of HNO_3 per unit volume of the system. All gases are assumed ideal, and the volume occupied by the liquid particles is neglected. Under these assumptions, the depletion of species i from the gas phase in the presence of a particle number concentration N_p of particles per unit volume is expressed as follows:

$$p_{\infty,i}(m_i) = p^0_{\infty,i} - N_\mathrm{p}\frac{R\,T}{M_i} m_i, \tag{2}$$

where $p^0_{\infty,i}$ denotes the initial vapor pressure in the atmosphere and the M_i are the molar masses. In the equilibrium calculations only $p_{\infty,\mathrm{HNO_3}}$ is constrained. For each fixed $m_{\mathrm{H_2O}}$, the HNO_3(g) is equilibrated with the particle. The water equilibrium vapor pressure over the resulting particle is then calculated from Eq. (1). Finally, the particle diameter is determined from the total mass and the composition-dependent density.

B. Thermodynamic model for the ternary $H_2O - HNO_3 - NH_4NO_3$ solution

The submodel "model II" of the E-AIM of Clegg and coworkers[17–19] is used to calculate the physical properties of the ternary watery solution of HNO_3 and NH_4NO_3, including the composition-dependent equilibrium vapor pressures over the flat solution and density $\rho(T_\mathrm{p}, \boldsymbol{m}_j)$ of the solution. The partial molecular volumes of water and HNO_3 in the liquid phase are also obtained from the density estimations provided by the E-AIM model, via the relationship

$$v_i = \frac{M_i}{N_\mathrm{A}}\frac{\partial V_\mathrm{p}}{\partial m_i} = \frac{M_i}{N_\mathrm{A}}\frac{\partial}{\partial m_i}\left(\frac{m_{\mathrm{H_2O}} + m_{\mathrm{HNO_3}} + m_{\mathrm{NH_4NO_3}}}{\rho(T_\mathrm{p}, \boldsymbol{m}_j)}\right), \tag{3}$$

where N_A is the Avogadro number and V_p the particle volume.

The latent heat of evaporation q_i of each species with respect to flat solutions is obtained from the equilibrium vapour pressures using the Clausius–Clapeyron equation

$$\mathrm{d}\ln(p_i) = -\frac{\Delta H_\mathrm{evap}}{R}\mathrm{d}\left(\frac{1}{T}\right), \tag{4}$$

$$q_i = \frac{\Delta H_{\mathrm{evap},i}}{M_i} = -\frac{RT^2}{M_i}\frac{\mathrm{d}p_i(T, \boldsymbol{m}_j)}{p_i(T, \boldsymbol{m}_j)\mathrm{d}T}, \tag{5}$$

where $p_i(T, \boldsymbol{m}_j)$ is the equilibrium vapor pressure of species i with particles of composition defined by the $\boldsymbol{m}_j$. In this expression, the correction factor for the Kelvin effect is neglected, since it remains below 1% over the whole considered size range.

C. Kinetic simulation: Model for the growth of ternary $H_2O - HNO_3 - NH_4NO_3$ particles driven by binary condensation of water and HNO_3(g)

In the approximation that the mass fluxes of water and of HNO_3 to the particle are independent from each other, the temporal evolution of the partial condensed masses m_i are governed by

$$\frac{\mathrm{d}m_i}{\mathrm{d}t} = \frac{2\pi\, D_i(T)\, M_i\, D_\mathrm{p}(T_\mathrm{p}, \boldsymbol{m}_j)}{R}\, f(Kn, \alpha_{\mathrm{m},i}) \times \left(\frac{p_{\infty,i}}{T_\infty} - \frac{p_{\mathrm{sat},i}}{T_\mathrm{p}}\, \exp\left[\frac{4\,\sigma\, v_i}{k_\mathrm{B}\, T_\mathrm{p}\, D_\mathrm{p}(T_\mathrm{p}, \boldsymbol{m}_j)}\right]\right). \tag{6}$$

In this equation, D_i the diffusivity of species i in air and T_∞ is the background temperature. The temperature variation of a particle is coupled to the mass change rates by the latent heat released or consumed, and by heat diffusion according to[20]

$$\frac{\mathrm{d}T_\mathrm{p}}{\mathrm{d}t} = \frac{q_{\mathrm{H_2O}}\frac{\mathrm{d}m_{\mathrm{H_2O}}}{\mathrm{d}t} + q_{\mathrm{HNO_3}}\frac{\mathrm{d}m_{\mathrm{HNO_3}}}{\mathrm{d}t} - 2\pi D_\mathrm{p}\, f(\mathrm{Kn}, \alpha_\mathrm{T})\, k_{air}(T_\mathrm{p} - T_\infty)}{c_\mathrm{sol}(m_{\mathrm{H_2O}} + m_{\mathrm{HNO_3}} + m_{\mathrm{NH_4NO_3}})}, \tag{7}$$

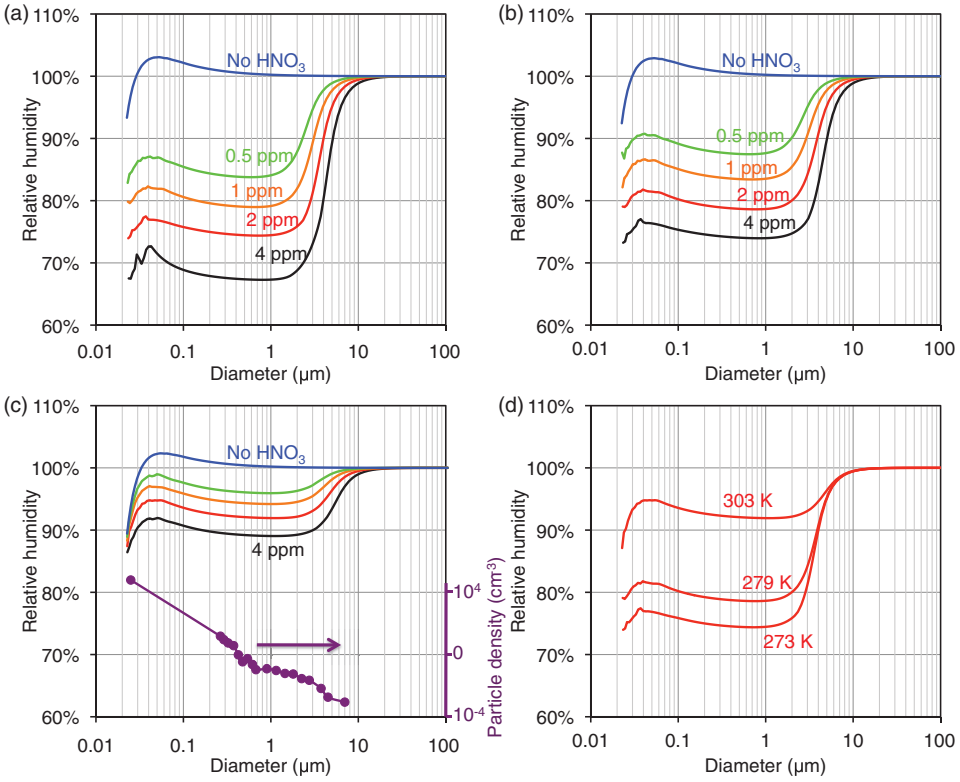

FIG. 1. (a–c) Köhler curves at 1 bar and (a) $T = 273$ K; (b) $T = 279$ K; (c) $T = 303$ K, for HNO_3 concentrations ranging from 0 to 4 ppm, as marked on the curves. (d) Temperature dependence of the Köhler plot for 2 ppm HNO_3(g). Particles have a NH_4NO_3 core of 15 nm diameter. Particle number concentration is $C_p = 1000$ cm^{-3}. The typical effect of the laser on the particle density, as observed in recent experiments (Ref. 5), is displayed for reference at the bottom of panel (c).

where c_{sol} is the specific heat capacity of the liquid phase and k_{air} is the thermal conductivity of air. The functions $f(\mathrm{Kn}, \alpha)$ are the Fuchs–Sutugin correction factors which account for the fact that the mean free path λ_i of gases in air is not negligible as compared to the particle size:[11]

$$f(\mathrm{Kn}, \alpha) = \frac{0.75\,\alpha\,(1 + \mathrm{Kn})}{\mathrm{Kn}^2 + \mathrm{Kn} + 0.283\,\alpha\,\mathrm{Kn} + 0.75\,\alpha}, \tag{8}$$

where $\mathrm{Kn} = 2\lambda_i / D_p$ is the Knudsen number,

$$\lambda_i = \frac{3 D_i}{\bar{c}_i} \tag{9}$$

and $\bar{c}_i$ is the mean thermal velocity of the vapor molecules in air

$$\bar{c}_i = \left(\frac{8\,k_B\,T}{\pi\,m_i}\right)^{1/2}. \tag{10}$$

Following the argument of Winkler *et al.*[21] and Laaksonen *et al.*,[22] the mass and thermal accommodation coefficients are assumed to be $\alpha = 1$. Furthermore, the values of D_i and k_{air} are taken from the literature.[11,20,23]

Using again the E-AIM Model II[17–19] for the ternary solution $H_2O - HNO_3 - NH_4NO_3$, we integrate the coupled time-dependent changes of water and HNO_3 partial masses

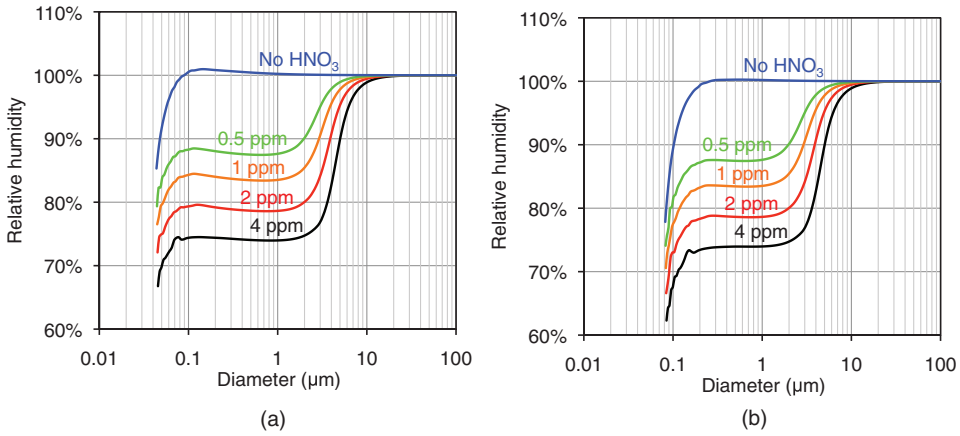

FIG. 2. Same as Fig. 1(b), with a dry salt diameter of (a) 30 nm and (b) 60 nm.

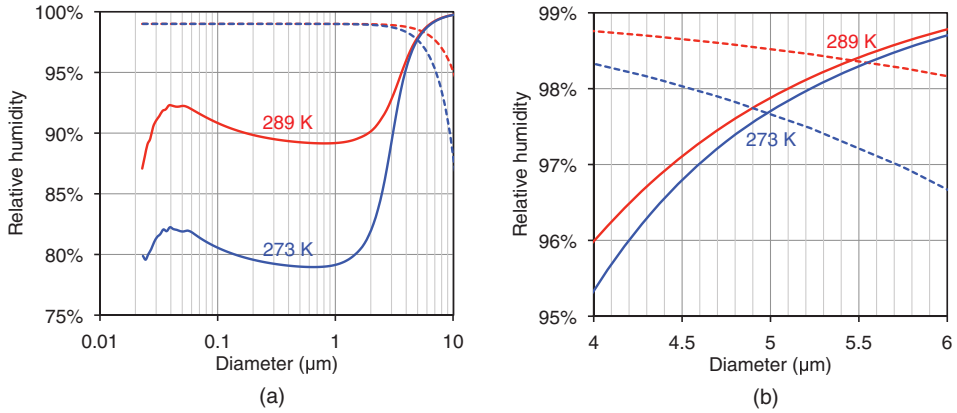

FIG. 3. Effect of water vapor depletion on particle growth for 2 ppm initial HNO_3(g) concentration, a 15 nm dry diameter NH_4NO_3 core, $C = 1000$ particles cm^{-3}, 99% initial RH, and 1 bar atmospheric pressure (a). Blue: $T = 273.15$ K; red: $T = 289$ K. Solid lines: Köhler curves; dashed lines: depletion-limited RH. (b) Linear scale closeup of the intersection region.

in the mixed particle liquid phase. Since our model does not describe the particle nucleation phase, the initial diameter is determined to ensure the equilibrium with the considered RH in the absence of HNO_3.

III. RESULTS

A. Particle stability

Figures 1(a) through 1(c) display the Köhler plots for temperatures and initial background HNO_3(g) vapor pressures covering the range of the reported experimental results.[5] These curves define, for the considered conditions, the relative humidity ensuring the stability of a particle as a function of its diameter. The addition of HNO_3(g) vapor drastically affects the shape of the Köhler crves. In particular, the RH required to quasi-activate (in the sense of Ref. 14) particles between 50 nm and 2 μm approximately, decreases strongly. As a consequence, two ranges of stable sizes (corresponding to positive slopes of the Köhler curves) emerge at RH values well below 100%, around 20–30 nm and several micrometers, respectively. This reduction of the RH ensuring quasi-activation of the particles is more pronounced for larger HNO_3 concentrations and low temperatures (Fig. 1(d)). While at $T = 273$ K a concentration of 4 ppm of HNO_3(g) is sufficient to depress the plateau below 70% RH, this threshold is close to 90% RH at $T = 303$ K.

Above 2 μm diameter, the Köhler curves steeply rise and progressively converge together between 4 and 10 μm, independent from the initial HNO_3(g) concentration.

The experimentally unknown diameter of the salt core has a minimal influence on our results. Doubling (Fig. 2(a)) or quadrupling (Fig. 2(b)) its diameter as compared with the conditions of Fig. 1(b), i.e., increasing the salt concentration by a factor of 8 and 64, respectively, only shifts the first activation barrier to slightly larger diameters and erodes the associated local maximum.

Köhler curves depict the static stability of the particles, and cannot give direct information about the depletion of water vapor. Still, this depletion can be evidenced indirectly on this basis by considering the evolution of the humidity in an atmosphere with initially 99% RH around monodisperse particles of diameter D_p that would grow while following the Köhler curve (Fig. 3). The dashed lines display the corresponding evolution of the RH. It is insensitive to the particle growth below ~ 2 μm, for which the condensed mass is negligible as compared to the total water mass. Beyond, the RH is depleted, so that the maximum particle size is defined by the point at which the atmospheric depletion brings the RH down to that required to ensure the particle stability.

B. Particle growth

The above-described particle growth along the Köhler curve is not physical, because the water vapor pressure would be in large excess of its equilibrium value (designated by the Köhler curve) most of the time. Furthermore, even with this approach, the Köhler curves give no kinetic information. Still, kinetic aspects are of key importance for efficient laser-induced condensation, which requires that the particles grow within a reasonable time. As is clearly visible in Fig. 4, particles grow fast over the wide range of considered conditions. Their size has already increased significantly after only 1 ms. They reach the micrometer-range within 100 ms, and stabilize between 4 μm and 8 μm after less than 10 s. These time constants are much faster than natural processes.[11]

Figure 4 also illustrates the influence of the initial conditions in the particle growth. For example, for 75% RH and 2 ppm HNO_3, the initially growing nucleus encounters the first ascending slope of the Köhler curve, left of its maximum. Since the RH is too low to allow the system to overcome the first maximum of the Köhler plot, a stable equilibrium is established at a particle diameter $D_p \approx 50$ nm.

The dynamics of matter exchange between the atmosphere and the growing particles is illustrated in Fig. 5. In the early stages of growth, HNO_3 accumulates fast in the particles, where its concentration rises until $t \approx 10$ ms. At this point, efficient water uptake from the gas phase begins, resulting in a relative dilution of HNO_3, hence in a slight decrease of its concentration until the end of the growth. Note that a similar growth sequence is observed in all conditions where particles grow, although the concentrations and time constants depend on the particle environment.

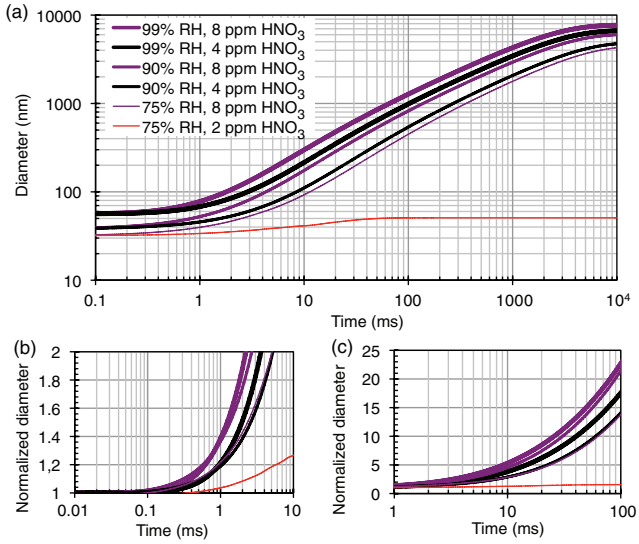

FIG. 4. Growth of the particle diameter for a temperature $T = 275$ K, an ammonium nitrate aerosol particle of dry diameter $D_{p,dry} = 25$ nm, and a particle number concentration $C_p = 1000\ cm^{-3}$. (b and c) Semi-logarithmic close-ups displaying the diameter relative to the initial one, (i.e. the relative growth speeds) on the time ranges where (b) HNO_3(g) and (c) water vapor uptakes dominate the particle growth (see Fig. 5).

IV. DISCUSSION

The timescale of the order of a second obtained in the model for the growth to (sub-) micrometer size is compatible with the *in situ* observations of filament-induced particle formation using the sampling particle counters.

At temperatures close to 0°C, a few ppm of $HNO_3(g)$ are sufficient to explain the lowering of the first activation barrier well below 100% RH. The efficiency of this process, however, decreases with increasing temperature, completely vanishing slightly above 30 °C. The proposed mechanism can, therefore, be expected to contribute substantially to laser-induced condensation under all temperature conditions, with more efficiency in cold weather conditions, as was observed in experiments.[5]

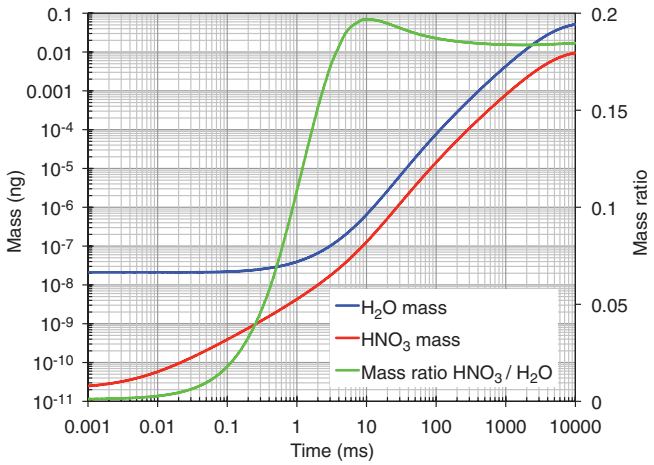

FIG. 5. Condensed masses of water and HNO_3 for $T = 275$ K and an initial HNO_3(g) concentration of 4 ppm. The ratio of dissolved HNO_3 and liquid water increases mainly during the initial 10 ms, and then remains below 20% in mass.

The temperature also indirectly influences the growth limit for big particle through its impact on the water vapor volume mixing ratio (VMR) for a given RH, via the Clausius–Clapeyron equation. Consequently, a higher water VMR allows the growth of larger particles. Similarly, the height of the first activation barrier raises with increasing temperature (Fig. 1(d)), so that fewer small particles can overcome it and grow up to the second barrier. With less activated particles, the competition between them to consume the water vapor and HNO_3(g) is less intense, so that each particle will be able to grow to larger sizes, since the available amount of water (and HNO_3(g)) will be distributed between less particles. This effect also explains the seemingly paradoxical negative correlation of RH with the concentration of large particles observed in experiments.[5]

Conversely, the laser-induced particle stabilization depends only weakly on the HNO_3 concentration in the atmosphere. Doubling this concentration appears to offset the Köhler curves by an almost constant amount, suggesting that the corresponding dependence is logarithmic and hence saturates beyond a few ppm. Due to this quite flat dependence, a precise knowledge of the HNO_3 concentration in the filaments or on their dilution influences the model only marginally, which makes it more robust relative to this hardly accessible parameter.

V. CONCLUSION AND OUTLOOK

As a conclusion, we have modelled the laser filament-induced particle stability and growth, based on the consideration of the extremely high HNO_3 concentrations (in the ppm range) generated within the filaments. This model offers a reasonable agreement with the published experiments[5] regarding both the sizes achieved by the particles and the fast growth speed. This agreement indicates that the stabilization of particles by HNO_3 solvation can explain a substantial part of the laser effect in filament-assisted condensation under a wide range of tempered atmospheric conditions. In this regard, the temperature appears as the most critical parameter, since the laser loses it effect above ~30 °C. Conversely, the HNO_3 concentration in the air has only a moderate influence on the cut-off size of the Köhler plot.

Finally, we have to keep in mind that our model is simplified, focusing on the role of HNO_3 alone. Quantitatively reproducing the experiments would require to consider polydisperse size distributions, the influence of H_2SO_4 produced by the laser by oxidizing the background atmospheric SO_2,[11,24–26] or charge-accelerated coagulation of particles of sub-100 nm size, which could explain the fast appearance of micrometer-sized particles per cm^3 of air. Moreover, owing to the fast particle growth predicted by the model, the assumption of a steady state, with constant flux of water vapor, may be questioned.

Furthermore, a full understanding of laser-induced condensation would require to consider not only particle growth, but also their nucleation. Besides H_2SO_4 and HNO_3, particle formation may be influenced by the charges released by the filaments, in a process similar to that at play in the Wilson chamber.[27,28] It is also probably influenced by the availability

of mineral or organic condensation nuclei, which may be activated and made hygroscopic[29–31] by the laser-generated ozone or HNO_3.[9,11] Although far beyond the scope of the present work, these physical mechanisms are obviously required to provide a full modelling of laser-assisted condensation.

ACKNOWLEDGMENTS

This work was supported by the Swiss NSF (Grants No. 20021-125315 and NCCR MUST program).

[1]S. L. Chin, S. A. Hosseini, W. Liu, Q. Luo, F. Théberge, N. Aközbek, A. Becker, V. P. Kandidov, O. G. Kosareva, and H. Schröder, Can. J. Phys. **83**, 863 (2005).
[2]L. Bergé, S. Skupin, R. Nuter, J. Kasparian, and J. Wolf, Rep. Prog. Phys. **70**, 1633 (2007).
[3]A. Couairon and A. Mysyrowicz, Phys. Rep. **441**, 47 (2007).
[4]J. Kasparian and J. Wolf, Opt. Express **16**, 466 (2008).
[5]S. Henin, Y. Petit, P. Rohwetter, K. Stelmaszczyk, Z. Hao, W. Nakaema, A. Vogel, T. Pohl, F. Schneider, and J. Kasparian, Nat. Commun. **2**, 456 (2011).
[6]I. Langmuir, Science **106**, 505 (1947).
[7]P. Béjot, J. Kasparian, S. Henin, V. Loriot, T. Vieillard, E. Hertz, O. Faucher, B. Lavorel, and J. Wolf, Phys. Rev. Lett. **104**, 103903 (2010).
[8]P. Béjot, E. Hertz, B. Lavorel, J. Kasparian, J. Wolf, and O. Faucher, Phys. Rev. Lett. **106**, 243902 (2011).
[9]Y. Petit, S. Henin, J. Kasparian, and J. Wolf, Appl. Phys. Lett. **97**, 021108 (2010).
[10]M. Chiwa, H. Kondo, N. Ebihara, and H. Sakugawa, Environ. Monit. Assess. **140**, 349 (2008).
[11]J. Seinfeld and S. Pandis, *Atmospheric Chemistry and Physics*, 2nd ed. (Wiley, Hoboken, NJ, 2006).
[12]Y. Petit, S. Henin, J. Kasparian, J. P. Wolf, P. Rohwetter, K. Stelmaszczyk, Z. Q. Hao, W. M. Nakaema, L. Wöste, A. Vogel, T. Pohl, and K. Weber, Appl. Phys. Lett. **98**, 041105 (2011).
[13]P. Konopka and W. Vogelsberger, J. Geophys. Res. **102**, D16057–16064 (1997)
[14]A. Laaksonen, P. Korhonen, M. Kulmala, and R. Charlson, J. Atmos. Sci. **55**, 853 (1998).
[15]H. Kokkola, S. Romakkaniemi, and A. Laaksonen, Atmos. Chem. Phys. **3**, 581 (2003).
[16]R. Jaenicke, in *Aerosol–Cloud–Climate Interactions* (Academic, Burlington, MA, 1993), pp. 1–31.
[17]S. L. Clegg, P. Brimblecombe, and A. S. Wexler, J. Phys. Chem. A **102**, 2137 (1998).
[18]C. Dutcher, A. S. Wexler, and S. L. Clegg, J. Phys. Chem. A **114**, 12216 (2010).
[19]S. L. Clegg and A. S. Wexler, J. Phys. Chem. A **115**, 3393 (2010).
[20]H. Pruppacher and J. Klett, *Microphysics of Clouds and Precipitation*, 2nd ed. (Kluwer, Dordrecht, 1997).
[21]P. Winkler, A. Vrtala, P. Wagner, M. Kulmala, K. Lehtinen, and T. Vesala, Phys. Rev. Lett. **93**, 075701 (2004).
[22]A. Laaksonen, T. Vesala, M. Kulmala, P. Winkler, and P. Wagner, Atmos. Chem. Phys. **5**, 461 (2005).
[23]J. Durham and L. Stockburger, Atmos. Environ. **20**, 559 (1986).
[24]F. Yu and R. Turco, Geophys. Res. Lett. **28**, 155 (2001).
[25]F. Yu, Atmos. Chem. Phys. **6**, 5193 (2006).
[26]J. Duplissy, M. B. Enghoff, K. L. Aplin, F. Arnold, H. Aufmhoff, M. Avngaard, U. Baltensperger, T. Bondo, R. Bingham, K. Carslaw, J. Curtis, A. David, B. Fastrup, S. Gagné, F. Hahn, R. G. Harrison, B. Kellett, J. Kirkby, M. Kulmala, L. Laakso, A. Laaksonen, E. Lillestol, M. Lockwood, J. Mäkelä, V. Makhmutov, N. D. Marsh, T. Nieminen, A. Onnela, E. Pedersen, J. O. P. Pedersen, J. Polny, U. Reichl, J. H. Seinfeld, M. Sipilä, Y. Stozhkov, F. Stratmann, H. Svensmark, J. Svensmark, R. Veenhof, B. Verheggen, Y. Viisanen, P. E. Wagner, G. Wehrle, E. Weingartner, H. Wex, M. Wilhelmsson, and P. M. Winkler, Atmos. Chem. Phys. **10**, 1635 (2010).
[27]C. Wilson, Philos. Trans. R. Soc. London Ser. A **192**, 403 (1899).
[28]F. Farley, Proc. R. Soc. London Ser. A **207**, 527 (1951).
[29]B. Wyslouzil, K. Carleton, D. Sonnenfroh, W. Rawlins, and S. Arnold, Geophys. Res. Lett. **21**, 2107 (1994).
[30]A. Vlasenko, S. Sjogren, E. Weingartner, K. Stemmler, H. Gäggeler, and M. Ammann, Atmos. Chem. Phys. **6**, 2147 (2006).
[31]A. Schwier, N. Sareen, T. Lathem, A. Nenes, and V. F. McNeill, J. Geoophys. Res. **116**, D16202 (2011).